

PHILOSOPHICAL TRANSACTIONS OF THE ROYAL SOCIETY B

BIOLOGICAL SCIENCES

When the Human Brain Goes Diving: Using NIRS to Measure Cerebral and Systemic Cardiovascular Responses to Deep, Breath-Hold Diving in Elite Freedivers

Journal:	<i>Philosophical Transactions B</i>
Manuscript ID	RSTB-2020-0349.R2
Article Type:	Research
Date Submitted by the Author:	04-Mar-2021
Complete List of Authors:	McKnight, J.Chris; University of St Andrews, Sea Mammal Research Unit Mulder, Eric; Mid Sweden University Campus Ostersund Ruesch, Alexander; Carnegie Mellon University, Department of Biomedical Engineering Kainerstorfer, Jana; Carnegie Mellon University, Department of Biomedical Engineering Wu, Jingyi; Carnegie Mellon University Hakimi, Naser; Artinis Medical Systems BV Balfour, Steve; University of St Andrews Sea Mammal Research Unit, SMRU Instrumentation Group Bronkhorst, Mathijs; Artinis Medical Systems BV Horschig, Jorn; Artinis Medical Systems BV Pernett, Frank; Mid Sweden University Campus Ostersund Sato, Katsufumi; Atmosphere and Ocean Research Institute, The University of Tokyo, International Coastal Research Center Hastie, Gordon; University of St Andrews, Sea Mammal Research Unit Tyack, Peter; University of St Andrews, Biology Schagatay, Erika; Mid Sweden University Campus Ostersund
Issue Code (this should have already been entered and appear below the blue box, but please contact the Editorial Office if it is not present):	MEASURING
Subject:	Physiology < BIOLOGY
Keywords:	NIRS, Freediving, breath-hold diving, Spo2, cerebral oxygenation, diving physiology

SCHOLARONE™
Manuscripts

Author-supplied statements

Relevant information will appear here if provided.

Ethics

Does your article include research that required ethical approval or permits?:

Yes

Statement (if applicable):

Scientific procedures involving freedivers complied with the Helsinki agreement and were approved by the Regional Committee for Medical and Health Research Ethics (Dnr 2019-05147). . Procedures for capture, handling, and housing of animals conformed to the Animals (Scientific Procedures) Act 1986, under the Sea Mammal Research Unit's Home Office licence (#70/7806) and were performed by personnel deemed competent under EU directive of the protection of animals used for scientific purposes.

Data

It is a condition of publication that data, code and materials supporting your paper are made publicly available. Does your paper present new data?:

Yes

Statement (if applicable):

All seal data and all code will be uploaded to the Dryad data repository on acceptance of the manuscript. Human data cannot be provided due to conflict with Ethical approval and potential breaches in anonymity due to the exceptional diving depths and durations reached.

Conflict of interest

I/We declare we have no competing interests

Statement (if applicable):

CUST_STATE_CONFLICT :No data available.

Authors' contributions

This paper has multiple authors and our individual contributions were as below

Statement (if applicable):

J. Chris McKnight: Conceptualisation, Methodology, Software, Formal analysis, Investigation, Data Curation, Writing, Visualisation. Eric Mulder: Investigation, Writing " Review and Editing, Project administration. Alexander Ruesch: Software, Formal analysis, Investigation, Visualisation, Writing. Jana Kainerstorfer: Conceptualisation, Methodology, Software, Writing. Nasar Hakimi: Software, Writing " Original Draft. Jingyi Wu: Software, Formal Analysis, Writing Original Draft. Steve Balfour: Methodology, Resources, Writing " Review and Editing. Mathijs Bronkhorst: Methodology, Resources, Writing. Jörn M. Horschig: Software, Formal analysis, Resources and Writing - Review and Editing. Frank Parnett: Data interpretation and writing. Katsufumi Sato: Resources and Writing " Review and Editing. Gordon D. Hastie: Resources, Writing " Review and Editing, and Funding acquisition (seal data). Peter Tyack: Resources and Writing " Original Draft.

1
2
3
4
5
6
7
8
9
10
11
12
13
14
15
16
17
18
19
20
21
22
23
24
25
26
27
28
29
30
31
32
33
34
35
36
37
38
39
40
41
42
43
44
45
46
47
48
49
50
51
52
53
54
55
56
57
58
59
60

Erika Schagatay: Conceptualization, Resources and contacts, Data interpretation and Writing, Project Administration and Funding acquisition (human data).

For Review Only

When the Human Brain Goes Diving: Using NIRS to Measure Cerebral and Systemic Cardiovascular Responses to Deep, Breath-Hold Diving in Elite Freedivers

Authors: J. Chris McKnight^{1,2*}, Eric Mulder², Alexander Ruesch³, Jana Kairnerstorfer³, Jingyi Wu³, Naser Hakimi⁴, Steve Balfour⁵, Mathijs Bronkhorst⁴, Jörn M. Horschig⁴, Frank Pernet², Katsufumi Sato⁶, Gordon D. Hastie¹, Peter Tyack¹ and Erika Schagatay²

Affiliations:

¹Sea Mammal Research Unit, Scottish Oceans Institute, University of St. Andrews, St. Andrews, Scotland.

²Department of Health Sciences, Mid Sweden University, Östersund, Sweden.

³Department of Biomedical Engineering, Carnegie Mellon University, 5000 Forbes Avenue, Pittsburgh, PA 15213, USA

⁴Artinis Medical Systems BV, Einsteinweg 17, 6662 PW Elst, The Netherlands.

⁵Sea Mammal Research Unit Instrumentation Group, Scottish Oceans Institute, University of St. Andrews, St. Andrews, Scotland.

⁶Atmosphere and Ocean Research Institute, The University of Tokyo, 5-1-5 Kashiwanoha, Kashiwa, Chiba 277-8564, Japan

Correspondence: jcm20@st-andrews.ac.uk

Abstract

Continuous measurements of hemodynamic and oxygenation changes in free-living animals remain elusive. However, developments in biomedical technologies may help to fill this knowledge gap. One such technology is continuous-wave near-infrared spectroscopy (CW-NIRS) - a wearable and non-invasive optical technology. Here we develop a marinized CW-NIRS system and deploy it on elite competition freedivers to test its capacity to function during deep freediving to 107 m depth. We use the oxy- and deoxy-haemoglobin concentration changes measured with CW-NIRS to monitor cerebral haemodynamic changes and oxygenation, arterial saturation and heart rate. Furthermore, using concentration changes in oxyhemoglobin engendered by cardiac pulsation, we demonstrate the ability to conduct additional feature exploration of cardiac dependant hemodynamic changes. Freedivers showed cerebral hemodynamic changes characteristic of apnoeic diving, while some divers also showed considerable elevations in venous blood volumes close to the end of diving. Some freedivers also showed pronounced arterial deoxygenation, the most extreme of which resulted in an arterial saturation of 25%. Freedivers also displayed heart rate changes that were comparable to diving mammals both in magnitude and patterns of change. Finally, changes in cardiac waveform associated with heart rates <40 bpm were associated with changes indicative of a reduction in vascular compliance. The success here of CW-NIRS to non-invasively measure a suite of physiological phenomenon in a deep-diving mammal highlights its efficacy as a future physiological monitoring tool for human freedivers as well as free-living animals.

1. Introduction

Central to the capacity for repeated or prolonged breath-hold diving in animals, such as seals and humans, is the suite of cardiovascular responses, collectively termed the 'diving response', that serve to conserve oxygen by down-regulating its rate of consumption [1,2]. Upon submersion, diving mammals respond with a significant redistribution of blood achieved through peripheral arterial constriction, preferentially distributing most of the cardiac output to

1
2
3 47 high-priority tissues such as the brain, heart, adrenals, and splanchnic organs [3,4]. The
4 48 consequent increase in peripheral resistance is compensated by a simultaneous and significant
5 49 reduction in heart rate, moderately reduced stroke volume, and reduced myocardial
6 50 contractility; matching left ventricular output to the restricted vascular beds and decreased
7 51 venous return [4,5]. Although these cardiovascular adjustments to diving reduce the rate of
8 52 blood oxygen depletion, extending aerobic dive duration for diving animals [6] promoting
9 53 efficient foraging, and prolonging apnea duration in humans [7], up to now their study has been
10 54 mainly limited to measurements in the laboratory. Human underwater foragers successfully
11 55 freedive repeatedly to 20 m for hours daily with dive durations under one minute [7], and
12 56 competition freedivers can perform static breath-holds lasting over 10 minutes, swim 300 m
13 57 underwater and – perhaps most remarkably - reach depths in excess of 100 m during swimming
14 58 dives lasting over 4 minutes (www.aidainternational.org). Sharing many physiological features
15 59 with consummate diving mammals [7], these deep human freedivers can potentially serve as a
16 60 tractable generalised model for work on diving mammals.

17
18
19
20 61 Despite extensive knowledge on the mechanistic drivers and moderating factors of the diving
21 62 response [3], how the fundamental components of the response, such as tissue-specific
22 63 perfusion and oxygenation, vary across tissues between dives and species during free-ranging
23 64 diving, and its impact on blood gas tensions and gas management is limited. Much of our
24 65 understanding of arterial or venous blood oxygenation in diving animals, including humans, is
25 66 based on haematological variables from the major vasculature using implanted intravascular
26 67 oxygen sensors [8,9], or cross-sectional measurements [6,10,11]. Information at the level of
27 68 individual tissues, including haemodynamics and oxygenation changes, is even more limited
28 69 and predominately derived from cross-sectional measurements from lethally sampled animals
29 70 after forced dives [5,12], numerical modelling exercises [13] or simulated, controlled diving
30 71 experiments [14]. These data, and methods of data collection, have provided a vitally important
31 72 basis for our understanding of the hemodynamic and gas tension changes engendered by
32 73 breath-hold diving. However, continuous measurements of parameters of hemodynamic
33 74 changes and blood oxygenation remain elusive – particularly in deep diving animals [15,16].
34 75 Developing a greater capacity for continuous oxygenation and hemodynamic measurement is
35 76 important both for research, such as understanding potential vulnerabilities and consequences
36 77 of observed physiological responses to anthropogenic disturbance on diving animals [17]; and
37 78 for applied science, such as improving safety in human breath-hold diving [18]. Advances in
38 79 wearable biomedical equipment, such as continuous wave near-infrared spectroscopy (CW-
39 80 NIRS) may provide a critical tool in reducing this knowledge gap.

40
41
42
43
44 81 CW-NIRS is a non-invasive, optical-based technology that measures relative concentration
45 82 changes in oxy-haemoglobin ($\Delta\text{O}_2\text{Hb}$), deoxy-haemoglobin (ΔHHb) [19]. Changes in $\Delta\text{O}_2\text{Hb}$
46 83 and ΔHHb can provide high-resolution measurements of relative blood volume changes [20],
47 84 mixed arterial-venous tissue-specific haemoglobin oxygen saturation (TSI) [21], arterial
48 85 oxygen saturation (SpO_2) [22], as well as heart rate and information on cardiac waveform
49 86 (similar to photoplethysmography [23]).

50
51
52 87 Here we describe the application of a custom-developed spatially-resolved CW-NIRS tag
53 88 designed to function on deep diving humans which provide a useful diving model for a test of
54 89 CW-NIRS as a technology for physiological measurement in diving animals. We monitored
55 90 changes in cerebral blood volume, cerebral TSI, SpO_2 , heart rate and diving behaviour in elite
56 91 freedivers, deep-diving of their own volition at sea. Studying diving humans, we highlight the
57 92 capacity of CW-NIRS to collect a variety of high-resolution cardiovascular and
58 93 cerebrovascular data during deep dives and present these data, with some comparisons to
59 94 diving mammals, to demonstrate the utility of CW-NIRS both to understand human freediving

1
2
3 95 physiology and as a comparative diving physiology research tool that could assist in improving
4 96 our physiological understanding of animal ecophysiology.

6 97 **2. Methods**

7 98 **NIRS system.** An archival NIRS sensor, PortaDiver, was developed from an existing wearable
8 99 dual-wavelength CW-NIRS system for humans (PortaLite mini) that simultaneously uses the
9 100 modified Beer-Lambert law [31] and spatially resolved spectroscopy methods. Changes in the
10 101 concentration of ($\Delta\text{O}_2\text{Hb}$) and (ΔHHb) can be calculated from changes in light absorption using
11 102 the modified Beer-Lambert law, which describes optical absorption changes in a scattering
12 103 medium. Since the absolute chromophore concentration is unknown, relative values for O_2Hb
13 104 and HHb were measured as a change from the start of each dive in micromolar units per litre
14 105 of tissue ($\mu\text{mol}\cdot\text{L}^{-1}$). This allowed calculation of total Hb ($[\Delta\text{HbT}] = [\text{O}_2\text{Hb}] + [\Delta\text{HHb}]$) that
15 106 can be used as a proxy for changes in blood volume. Tissue saturation index (TSI) is a measure
16 107 of tissue oxygen saturation of haemoglobin (combined arterial and venous contribution,
17 108 measured using a modified diffusion equation and validated both *in vitro* and *in vivo* [24]) and
18 109 uses multiple channels to remove the contribution of non-cerebral tissue from the measurement
19 110 [25]. A Quality Control Factor (QCF) which estimates model fit was used to ensure TSI
20 111 reliability. The QCF is a correlation factor to indicate the quality of the measured slope, where
21 112 the value 1 is a perfect fit and 0 is no fit. TSI values with a QCF value lower than 99.9 were
22 113 removed from the dataset as these values are a result of insufficient contact between emitters
23 114 and/or receivers with skin.

24 115
25 116 NIRS measures a volume of tissue containing microvasculature, comprising capillary,
26 117 arteriolar, and venular beds but not large arteries and veins. The PortaLite mini consisted of a
27 118 sensor body, housed in an aluminium case with a removable O-ring sealed lid (with three
28 119 optical acrylic windows), and a sensor head. To waterproof the sensor head, the light diodes,
29 120 photodiode receiver, and printed circuit boards (PCBs) of the sensor head were first fitted into
30 121 optically opaque polyoxymethylene housings. The housings were filled with spectrally
31 122 transparent epoxy (EPO-TEK 301, Epoxy Technology, Billerica, MA, United States). To
32 123 ensure that epoxy encapsulated the electronics but did not cover the optical window on the
33 124 optodes, the sensor head was cradled in a custom-built silicone mould. This allowed the internal
34 125 components to be filled and waterproofed by epoxy but ensured the external surface and LEDs
35 126 remained exposed. Once the housings were filled with epoxy, an optically opaque lid was
36 127 placed onto the housing and fixed with two screws. Finally, the exterior of the housings and
37 128 interoptode were potted in optically transparent polyurethane for flexibility, allowing the
38 129 sensor head to conform to the shape of each divers head. Distance between light sources and
39 130 detector were 30 mm (850 nm and 751 nm optode), 35 mm (852 nm and 751 nm optode), and
40 131 40 mm (851 nm and 752 nm optode), allowing optical penetration to three different tissue
41 132 depths (larger spacing between the optode and receiver allows deeper optical penetration). The
42 133 response time of the PortaDiver was ≤ 0.1 s. The PortaDiver was controlled via a combination
43 134 of magnetic reed switches and Bluetooth allowing the system to be controlled from within the
44 135 waterproof housing without the necessity for opening. Following marinization of the
45 136 instrument, the device was returned to the manufacturer (Artinis Medical Systems BV) for
46 137 calibration, testing and approval of accurate functionality. The PortaDiver measured oxy-
47 138 haemoglobin ($\Delta\text{O}_2\text{Hb}$), deoxy-haemoglobin (ΔHHb) concentration changes, and cerebral
48 139 blood oxygen saturation index (TSI - expressed as a percentage). The NIRS data were used to
49 140 calculate changes in total haemoglobin ($[\Delta\text{HbT}] = \Delta\text{O}_2\text{Hb} + \Delta\text{HHb}$), arterial oxygen saturation
50 141 (SpO_2), and heart rate.

Swimming movements were measured with a Little Leonardo W1000-PD3GT (Little Leonardo, Tokyo, Japan), (Fig. S1A) which logged tri-axial acceleration (32Hz), depth (1Hz) and temperature (1Hz).

Fig. 1. Monitoring diving physiology and behaviour in elite freedivers. (A) Location of NIRS sensor-head over prefrontal cortex (red box). **(B)** Respective placements of NIRS sensor body (red box) and Little Leonardo W1000-PD3GT (yellow box).

Human diving trials. Five elite male competition freedivers, all active competitors, volunteered to participate during training dives. The PortaDiver and Little Leonardo W1000-PD3GT bio-logging devices were attached to a diver while onboard a boat before each recording session. The PortaDiver sensor body was placed inside the diver's wetsuit. The PortaDiver sensor head was inserted into the diver's wetsuit hood above the left eye, on the forehead over the pre-frontal cortex. The Little Leonardo was clipped to the diver's weight belt with low strength cable ties to ensure it would come away from the freedivers if the instrument became tangled. Divers were then operating of their own volition throughout their freediving training session. Safety divers were present during all dives. All divers used "lung packing" (glossopharyngeal insufflation) to fill lungs above normal total lung capacity before the start of each dive [26]. Dives were made during three depth competition disciplines; constant weight vertical swimming to depth using fins or a monofin (8 dives), constant weight swimming without fins (4 dives), and free immersion (5 dives) involving the diver manually pulling down and up on a rope using their arms (see Schagatay 2011 [7] for details). Once the divers had completed their training session and exited the water, the instruments were removed. Scientific procedures involving freedivers complied with the Helsinki agreement and were approved by the Regional Committee for Medical and Health Research Ethics (Dnr 2019-05147).

Seal NIRS data. To demonstrate the translatable capacity of NIRS from humans to diving animals, NIRS data, collected from a juvenile grey seal (*Halichoerus grypus*), were also included in the cardiac waveform analysis described below. Seal data were collected using a wearable NIRS device ('Brite24' Artinis Medical Systems BV, Einsteinweg, The Netherlands) with 16 dual-wavelength emitters and eight photodiode detectors, configured to provide 28 channels. The LED emitters each had two NIR light sources with wavelengths of 755-758nm and 839-854nm and the eight photodiode detectors had an incorporated ambient light filter. The optode-detector trace visualised had a separation distance of ~30mm (long channels). Data were collected on a juvenile grey seal anaesthetised using a combination of midazolam (Hypnovel, Roche Products Ltd, UK; 5 mg/ml solution, 0.03 ml/kg IM as a premedication sedative and 0.01 ml/kg IV to control tremors) and ketamine (Ketaset, Zoetis, UK 100 mg/ml solution, 0.01 ml/kg IV). Procedures for capture, handling, and housing of animals conformed to the Animals (Scientific Procedures) Act 1986, under the Sea Mammal Research Unit's Home Office licence (#70/7806) and were performed by personnel deemed competent under EU directive of the protection of animals used for scientific purposes.

Heart rate extraction. A heart rate derivation algorithm presented in [27] was applied to extract heart rate from the NIRS signal. The algorithm consists of three steps: (1) pre-processing, (2) heart rate extraction, and (3) heart rate correction. In the pre-processing step, a 100th order zero-phase bandpass FIR filter between 0.1 Hz and 4 Hz was applied. This

185 effectively reduces the influence of motion and systemic artefacts in the data and allows for
 186 more reliable heartbeat detection.

187 In the heart rate extraction step, the peak points in the pre-processed signal were detected by
 188 applying the AMPD method [28]. AMPD is an automatic peak detection algorithm applicable
 189 to noisy periodic and quasi-periodic signals. It is based on calculating and analyzing the local
 190 maxima scalogram which produces a matrix comprised of the scale-dependent occurrences of
 191 the local maxima. After applying the AMPD peak detection algorithm, the momentary heart
 192 rate is obtained by calculating the peak-to-peak time interval. The continuous heart rate signal
 193 is then constructed through cubic interpolation.

194 In the heart rate correction step, a windowing approach based on the method presented in [27]
 195 is used to reduce errors due to false alarms of peak detection. In this method, a permissible
 196 range is initially defined for each extracted heart rate value. The permissible range is distributed
 197 around the mean of the extracted heart rate of the previous 4 seconds (m) with a permissible
 198 deviation. The permissible deviation is created by a weighted ($k = 21$) ratio of the total
 199 standard deviation of the heart rate signal from the start to the present time (SD) to the standard
 200 deviation of the previous 4-seconds (sd). Extracted heart rates which fall outside of the
 201 permissible range ($m - k \times \frac{SD}{sd} < HR < m + k \times \frac{SD}{sd}$) are removed and the samples are
 202 interpolated using a cubic spline.

203 **Arterial Saturation (SpO₂) extraction.** Cardiac related pulsatile signals can be detected in
 204 different parts of the human body, including the finger, ear lobe and forehead by using NIRS
 205 monitoring. These pulsatile signals occur as a result of attenuation of light by the increase of
 206 arterial blood volume during systole in the cardiac cycle [29]. Consequently, the detected
 207 oscillations in the optical signal can be attributed to the arterial blood, with
 208 a saturation which is then related to the oscillatory components of the optical densities at two
 209 or more wavelengths. Pulse oximetry exploits these pulsatile signals to calculate oxygen
 210 saturation (SpO₂). We exploit this same principle here to calculate SpO₂ using NIRS
 211 [22,29,30]. Specifically, we employ the SpO₂ extraction methodology, validated against pulse
 212 oximetry measures of SpO₂, used by Menssen et al. [22]. SpO₂ extraction was performed in
 213 MATLAB [The MathWorks Inc., Natick, MA, USA], and the algorithm consisted of three
 214 steps: (1) preprocessing, (2) frequency spectrogram generation, and (3) SpO₂ calculation. In
 215 the preprocessing step, a 3rd order zero-phase Butterworth filter at 0.4Hz was applied to the
 216 measured ΔO_2Hb and ΔHb traces. Spectrograms of the filtered ΔO_2Hb and ΔHb were
 217 generated, from which heart rate variation over time can be observed. At a particular time point
 218 in the spectrogram, heart rate was identified by the peak frequency component and the spectral
 219 power of ΔO_2Hb and ΔHb at the frequency was extracted. SpO₂ was calculated using these
 220 values at each time point such that $SpO_2 = \Delta O_2HbHR / [\Delta O_2HbHR + \Delta HbHR]$. The
 221 extraction of SpO₂ requires the calculation of fast Fourier transforms (FFTs) in defined time
 222 bins, creating a spectrogram. The time bin size determines the resolution of the FFT and
 223 therefore the precision of the extraction of spectral power at the heart rate, which is the
 224 fundamental information for SpO₂ calculations. Typically, bin size of 10-35 seconds was used
 225 (mean = 26.3 seconds) over which one FFT was calculated and from which one SpO₂ value
 226 could be extracted. Because the SpO₂ value was assigned to the center time point of the time
 227 bin, no SpO₂ values could be calculated prior to half the bin size from the start and the end of
 228 the measurement.

229 **Cardiac waveform analysis by Pulse averaging in freedivers.** To investigate potential
 230 changes in cardiac waveform and changes in heart rate associated with diving, and potentially
 231 indicative of changes in blood pressure and/or change in vascular compliance, analysis of the

232 pulse shape across cardiac cycles was analysed with particular attention focused on three
 233 waveform features: 1) percussive wave (originating from the contraction of the left ventricle
 234 and ejection of blood); (2) tidal wave (caused by the elasticity of aortic wall); (3) diastolic
 235 minimum (caused by full relaxation of the heart). Signal processing was performed using
 236 MATLAB. Raw light intensities were extracted, and the modified Beer-Lamberts law was
 237 applied [31]. This allowed the computation of zero-centred $[\Delta O_2Hb]$ and $[\Delta HHb]$ for every
 238 given source-detector combination; $[\Delta HbT]$ was calculated as the sum of $[\Delta O_2Hb]$ and
 239 $[\Delta HHb]$. Signals were visually inspected for movement artefacts, which were removed from
 240 the data. A high pass filter with a transition band of 0.1 Hz to 0.2 Hz was used to remove
 241 baseline drifts.

242 The data were upsampled from 10Hz to 100Hz sampling frequency. The peak finding
 243 algorithm was then applied to the first derivative of the $[\Delta HbT]$, as this proved to be more
 244 robust than a direct peak finding of the diastolic valley. The search parameters were similar to
 245 those described above for the seal, with a weighting factor of 0.5 for the minimum peak
 246 prominence and a minimum peak distance of 0.7 seconds. A time window between 0.5 s before
 247 and 2.9 seconds after the onset of every detected pulse was extracted and a moving average
 248 was applied. Fifteen consecutive pulses were averaged, to improve signal to noise ratios.
 249 Outliers were removed by z-score rejection. To identify the true diastolic minima, we first
 250 searched for all local minima in every cardiac pulse utilizing the 'islocalmin' function
 251 ('islocalmin', MATLAB). For every local minimum in the starting pulse, a tracking algorithm
 252 over time was implemented across all following pulses. The tracking was a search for the
 253 closest local minimum as compared to the previous pulse, with respect to the position in time
 254 in which the local minimum occurred ($T_{relative}$), the difference in height (H) and prominence
 255 (P) of the minimum as well as the distance in time to the first, original, diastolic minimum
 256 (T_{origin}). The search radius between 0.5 seconds before and 1 second after the previous local
 257 minimum was chosen. Peak heights and prominences were normalized to the systolic
 258 maximum of every pulse, making it a systolic peak height percentage. Time measurements
 259 were normalized to be a percentage of the total time of 2.9 seconds following the original
 260 diastolic valley. The best successor to the current local minimum was determined by the
 261 minimum of the error function $EF = T_{relative} + 2 T_{origin} + H - P$. Once the tracking of all
 262 local minima was complete, the algorithm was repeated starting from the last pulse going
 263 backwards to the first pulse. Finally, the most probable trace of local minima was determined
 264 to be the second diastolic valley in the signal by comparing goodness of fit function defined as
 265 $GOF = \bar{P} - \bar{H} - 1.5 \bar{T}_{origin}$, with \bar{P} as the average prominence in the trace, \bar{H} is the average
 266 valley height, and \bar{T}_{origin} the average time passed since the pulse onset. Waveforms were
 267 normalized in height and length to observe the pulse shape change independent of the change
 268 in heart rate and pulse height. The average diving depth and average heart rate for every pulse
 269 was determined. Pulses were then averaged in bins of 5 m diving depth or 10 bpm of heart rate,
 270 respectively.

271 **Cardiac waveform analysis by pulse averaging in the seal.** An elliptical high pass filter with
 272 a transition band between 0.2 Hz and 0.3 Hz was created ('ellip', MATLAB) and applied to
 273 the data through the phase preserving function 'filtfilt' ('filtfilt', MATLAB). The data were
 274 then upsampled from 10 Hz to 100 Hz using spline interpolation. In combination with a pulse
 275 averaging described below, this procedure allowed certain details from the cardiac pulsation
 276 beyond the low sampling frequency of 10Hz to be retained.

277 A direct peak finding approach on the inverted $[\Delta HbT]$ signal was then performed using the
 278 'findpeaks' function ('findpeaks', MATLAB) to determine diastolic minima in the signal.

279 Search parameters included a minimum peak prominence of one standard deviation of the
280 signal, divided by the square root of the upsampling ratio of 10, weighted by an empirically
281 determined factor of 0.2. The minimal peak distance was determined to be 0.5 seconds and the
282 minimum peak height was set to 0. A time window between 0.5 seconds before and 2.9 seconds
283 after, the found diastolic minimum was extracted. A moving average across 5 consecutive
284 pulses was then applied. To remove outliers caused by motion artefacts or failed diastolic
285 minima extraction, a z-score rejection across the pulses for every individual point in time was
286 applied. If at any given time a $z > 3$ was determined, the entire pulse was rejected. Fig. 4B
287 shows these averaged curves, zeroed to the first diastolic minimum and cut off after the second
288 diastolic minimum found in each individual averaged pulse.

289 3. Results

290 Data were successfully collected from each of the 17 dives made by the freedivers. Dives
291 ranged in duration from 49 to 249 s (mean = 130 s; standard deviation = ± 64 s) and ranged in
292 depth from 21 to 107 m (mean = 50 m; standard deviation = ± 26 m). All dives generated
293 continuous data, which could be analysed, while some loss of data occurred in the seconds
294 immediately before the divers surfaced. Insufficient contact between one NIRS channel and
295 the skin of the freedivers meant TSI could not be calculated for 4 dive (Table S1). Diving
296 profiles, cerebral hemodynamic responses, heart rate, cerebral and arterial blood oxygen
297 responses and temperature data are shown for two example dives, one CWT to 67 m and one
298 FIM dive to 97 m, in figure 2.

299
300 **Fig. 2. Monitoring physiological variables in freedivers.** Two example dives to 67 m
301 and 97 m from two freedivers, showing (A) Dive and temperature data (B) Cerebral
302 hemodynamic responses. (C) Heart rate, cerebral and arterial blood oxygen
303 responses. High-frequency peaks and troughs in the accelerometry signal are
304 indicative of leg movements associated with swimming in the CWT dive in example 1
305 and arm movements of pulling along the rope in a FIM dive in example 2. During early
306 descent the divers swim intensely to overcome positive buoyancy which is seen as
307 high amplitude peaks on the acceleration trace, while later during the descent the
308 negatively buoyant divers free-fall. At the bottom of the dive when the divers turn and
309 swim upwards against negative buoyancy, the acceleration trace, again, shows high
310 amplitude peaks throughout ascent. Oscillations in TSI from minutes 4 to 5 in example
311 2 were likely the result of involuntary breathing movements [14]. TSI measurement in
312 example 2 was lost on surfacing as one of three NIRS channels lost contact with the
313 diver's head.

314 Cortical Haemodynamic Responses

315 Continuous measurements of $[\Delta O_2Hb]$ and $[\Delta HHb]$ allowed the continuous changes in CBV,
316 cerebral TSI, and SpO_2 to be calculated for all 17 dives. $[\Delta O_2Hb]$ and $[\Delta HHb]$ showed little
317 change during pre-diving except for slow-wave oscillations while divers were still breathing.
318 However, immediately before diving, when divers performed 'lung packing' there was a
319 reduction in $[\Delta O_2Hb]$ with a consequent fall in CBV and TSI (as visible before the onset of

1
2
3 320 diving in Fig. 2). Upon diving $[\Delta O_2Hb]$ rose to exceed pre-diving levels, with a consequent
4 321 elevation in CBV above pre-diving levels and restoration of TSI to pre-lung packing levels
5 322 (Fig. 2).

7 323 Across the remainder of the diving period, patterns of change in $[\Delta O_2Hb]$ and $[\Delta HHb]$ varied
8 324 across dives and divers, which could be expected with different individuals performing dives
9 325 of differing depths, durations and disciplines. As demonstrated in Fig. 2B, two dives from
10 326 different divers show considerable differences in patterns of change in $[\Delta O_2Hb]$, $[\Delta HHb]$, and
11 327 $[\Delta HbT]$ over the diving period. In example dive one, cerebral haemodynamic changes resulted
12 328 in TSI remaining close or above pre-diving levels throughout the dive. However, in example
13 329 dive 2, while TSI remained high throughout the descent phase of the dive, it declined during
14 330 ascent and showed a marked increase in the rate of decline during the last 10-15 m as $[\Delta HHb]$
15 331 and CBV rose. This phenomenon of low TSI, concomitant with increased CBV engendered by
16 332 rising $[\Delta HHb]$, was seen in 8 of the 17 dives logged – all of which were the longest dives
17 333 performed by participants.

20 334 SpO_2 dynamics were similar across all dives. SpO_2 remained close to pre-diving levels (>95%)
21 335 during descent, before generally declining during ascent. Greater declines in SpO_2 were
22 336 observed during longer dives, with the lowest SpO_2 value recorded being 25% (Fig. 3A). On
23 337 longer dives, SpO_2 declines were generally concomitant with declines in TSI, except for the
24 338 previously described rapid drops in TSI in the last 10-15m of ascent.

27 339
28 340 **Fig. 3. (A)** Arterial oxygen saturation (SpO_2) and depth data from a dive resulting in
29 341 the lowest arterial blood oxygenation recorded (25%). **(B)** Heart rate and depth profiles
30 342 for a human diver (80kg) perform the deepest dive recorded (107 m) and an 81 kg
31 343 California sea lion (*Zalophus californianus*) diving to 240 m (data re-drawn with
32 344 permission from McDonald and Ponganis 2014 [32])

38 345 Cardiac Responses

39 346 Blood volume changes associated with cardiac pulsation (as measured here in the brain and
40 347 scalp of the freedivers), evident in the $[\Delta O_2Hb]$ signal (Fig. 4) and to a lesser extent in the
41 348 $[HHb]$ signal, allowed heart rate to be extracted for each of the 17 dives. Heart rate changes
42 349 across the period of diving showed a similar pattern across all dives. Following the onset of
43 350 diving, heart rate declined during the dive descent (Fig. 2C & 3B). Minimum heart rate was
44 351 reached at the bottom of the dive after a period of passive descent during “free fall”, before
45 352 showing an overall increase during ascent, especially during early ascent involving exercise to
46 353 overcome negative buoyancy (Figs 2C & 3A).

49 354
50
51 355 **Fig. 4. Raw $[O_2Hb]$ traces visualising heart rate and cardiac waveform. (A)** Shape and
52 356 magnitude of a normal cardiac waveform at 41bpm. **(B)** Cardiac waveform with
53 357 increased magnitude and pronounced tidal waves at a heart rate of 27bpm. **(C)**
54 358 Cardiac waveforms across four cardiac cycles with three key features identified – (1)
55 359 percussive wave (originating from the contraction of the left ventricle and ejection of
56 360 blood); (2) tidal wave (caused by the elasticity of aortic wall); (3) diastolic minimum

361 (caused by relaxation of heart) - showing the transient changes in cardiac waveform
362 on the longest interbeat interval (5.4 s) recorded.

363 The magnitude of reduction in heart rate across the descent phase of each dive was pronounced
364 and, in some cases, comparable in magnitude to diving mammals (Fig. 3B). As shown in Fig.
365 4B (red line), where a diver exhibits <27 beats over 60 s, sustained low heart rates were not
366 uncommon. Indeed, the longest interbeat interval measured in the current study was 5.4 s (Fig.
367 4C), representing a heart rate of 11 bpm. The high-quality cardiac pulsation signal within the
368 data allowed participants' cardiac waveforms to be analysed for potential changes associated
369 with diving. By performing cardiac waveform analysis on the cardiac pulsation signal it was
370 apparent that in nine of 17 dives, divers' cardiac waveforms showed progressive changes with
371 heart rate and depth – specifically, the height of the percussive peak (pulse magnitude) and the
372 prominence of the tidal peak both increased (Fig. 5A) at lower heart rates. Similar signal
373 analysis for heart rate extraction and cardiac waveform channel was performed on the seal data
374 to validate the transferability of the NIRS signal and signal-processing to marine mammals
375 (Fig. 5B). Similar to human data, at lower heart rates the example seal data showed increased
376 percussive peak height (pulse magnitude) (Fig. 5C) and greater prominence of the tidal peak
377 (Figs. 5A&B). Figs. 5D&E show participant waveforms normalized in height and length,
378 therefore independent of changes in heart rate, demonstrating that with both increased depth
379 and lowered heart rate (which themselves are correlated; Figs. 2&3B) there was greater
380 prominence in the tidal peak.

381
382 **Fig. 5. Cardiac pulsation of ΔHbT compared between a grey seal and human diver.**

383 The cardiac pulsation of ΔHbT for one example dive (A) is compared to the resting
384 state cardiac pulsation in a grey seal (B). The colour encodes the underlying heart
385 rate, revealing increasing pulse magnitude with bradycardia heart rate. (C) Comparing
386 the human diver from (A) and the grey seal in (B), the average ΔHbT (sum of oxy- and
387 deoxy-haemoglobin) magnitude, with errorbars spanning the standard deviation within
388 the 5 bpm interval in heart rate, reveals similar trends. The pulse shape change in the
389 human diver is emphasized by normalizing the pulses in length and height. Pulses are
390 then averaged based on the underlying diving depth (D) and heart rate (E), with
391 shaded error bars spanning the standard deviation of the normalized ΔHbT at any
392 given time of the pulse.

393 4. Discussion

394 The results presented here demonstrate the capacity of non-invasive CW-NIRS to function as
395 a physiological monitoring tool in trained human freedivers during diving to extreme depth.
396 Extremely low values for both heart rate and SpO_2 were recorded in these dives, as well as
397 variable cerebral haemodynamic pattern, and transient changes in cardiac waveform in some
398 divers. The capacity to simultaneously measure hemodynamic changes, and calculate tissue-
399 specific and arterial oxygenation, along with heart rate and cardiac waveform changes, show
400 that CW-NIRS has the potential to provide continuous high-resolution physiological changes
401 in naturalistic conditions for humans as well as other diving animals.

402 Cortical Haemodynamic Responses

403 Continuous measurements of tissue-specific haemodynamic changes in diving animals remain
404 elusive. However, the NIRS instrument in the current study successfully provided continuous
405 measurements of CBV and tissue-oxygenation, and suggests that NIRS could facilitate in
406 addressing this knowledge gap. Indeed, little is known about patterns of change in tissues, such
407 as the brain, in diving animals [4,12,20]; with no information on context specific-changes (i.e.,
408 deep high-exertion foraging dives vs shallow transiting dives) as measurements have been
409 restricted to predictable simulated foraging [20] or simulated diving [4,12] paradigms.
410 Importantly, in the current study it was clear that different divers, dive depths, diving
411 disciplines, and respiratory mechanics affected patterns of change in CBV and TSI.
412 Nevertheless, it is unknown whether such variability in diving CBV and TSI exists in other
413 diving mammals, how this could be affected by activity, nor how this may vary between
414 species. Even initial deployments of NIRS on vertically diving animals could provide
415 interesting new insights into cerebral haemodynamic and oxygenation changes.

416 In the current study, two phases of diving resulted in TSI deflections in the freedivers. Firstly,
417 during pre-diving lung-packing, and secondly, in the second half of long and deep dives. TSI
418 deflections during lung packing were driven by a reduction in $[\Delta O_2Hb]$ and CBV (Fig. 2B).
419 This may be the result of a reduction in cerebral blood flow through reduced arterial blood
420 pressure and cardiac output associated with the lung packing manoeuvre [33]. Reduced TSI in
421 the second half of longer and deeper dives resulted in marked reductions in end-dive cerebral
422 TSI values. Low end-dive TSI may not simply be a function of longer breath-holds, as the rapid
423 decline in TSI at the end of the dive was a function of increased cortical $[\Delta HbHb]$ but not
424 declining $[\Delta O_2Hb]$ (Fig. 2 example dive 2). Thus, elevated $[\Delta HbHb]$ and CBV does not appear
425 to solely be a product of diminishing SpO_2 , but also, potentially, hypercapnia affecting
426 haemoglobin oxygen affinity, as suggested by Dujic et al [14]; and elevated cerebral blood
427 flow via hypercapnia mediated increases in endogen catecholamines [34,35]. Investigating the
428 prevalence of this phenomenon across divers, diving depths/durations, and disciplines, as well
429 as the underlying drivers of this phenomenon, is worthy of future, targeted investigation.
430 Additionally, inclusion of control NIRS data from non-elite freedivers would be valuable in
431 assessing underlying impacts of variability in individuals' physiology, function of elite
432 conditioning or impact of factors such as NIRS probe placement. Nevertheless, dynamics such
433 as changes in the contribution to the NIRS signal from $[\Delta HbHb]$ close to the end of long dives,
434 and in some cases dramatic TSI changes with changes in respiratory mechanics before diving,
435 highlight additional information that CW-NIRS can provide alongside tissue-specific perfusion
436 changes.

437 SpO_2

438 Measurements of SpO_2 are not common in free-ranging animals, nor deep-diving humans,
439 particularly those derived through optical measurement. The successful extraction here of SpO_2
440 from the NIRS signal, in combination with CBV and cerebral TSI changes, is an informative
441 physiological combination – linking arterial blood oxygen delivery with tissue-specific blood
442 oxygenation and haemodynamics changes, which could be particularly interesting when
443 assessing cerebrovascular dynamics in breath-hold diving animals.

444 In all freedivers, SpO_2 remained high throughout the descent phase of each dive. Elevated
445 ambient pressure associated with descent and resultant elevated alveolar and arterial PO_2 serve
446 to maintain SpO_2 close to levels at the onset of the dive. Shortly after the start of the ascent
447 phase of each dive, SpO_2 began to decline and continued to do so throughout the remainder of
448 the dive. As ambient pressure declines during ascent, alveolar and arterial PO_2 decline causing
449 the reduction in SpO_2 . Elevated heart rate during early ascent, reflecting the enhanced exertion

1
2
3 450 when the diver swims up against negative buoyancy, increases cardiac output, which may also
4 451 affect the decline of SpO₂ [11]. As such, reperfusion of previously ischemic body
5 452 compartments elevating whole-body oxygen consumption rate, along with depth-specific
6 453 reduction in blood oxygen tension and/or exercise-induced stimulation tachycardia [3], could
7 454 also explain why the rate of decline in SpO₂ increased throughout ascent (Figs. 2 and 3A).
8 455 Interestingly, end-dive SpO₂ values on longer dives were at times below those experienced by
9 456 humans climbing mount Everest [36], with the lowest SpO₂ value recorded in the current study
10 457 at 25% (Fig. 3A) - a value normally not compatible with consciousness [7]. It should also be
11 458 noted that due to the FFT window size in the SpO₂ extraction process, the desaturation to 25%
12 459 SpO₂ was potentially exceeded before surfacing. This confirms that freedivers are at risk of
13 460 syncope during ascent, in line with the concept of “shallow water blackout” [18].

16 461 Cardiac Responses

17 462 As heart rate has been measured in several marine mammals and with application in energetics
18 463 assessments [37], a capacity to relate cardiac changes to arterial oxygenation and tissue-
19 464 specific hemodynamic and oxygenation changes via NIRS, could be useful for both
20 465 comparative physiological comparison and energetic measurements.

21 466 The overall patterns of change in heart rate in the freedivers were similar to those previously
22 467 reported for elite deep-freediving humans [38] and small/medium-sized marine mammals [32]
23 468 (Fig. 3). Following the onset of diving, heart rate dropped until the bottom of the dive (Fig. 2
24 469 & 3B). Elicitation of the diving response upon diving by apnea and stimulation of peripheral
25 470 facial receptors [3] results in bradycardia which maintains arterial blood pressure during
26 471 selective peripheral constriction, supporting the downregulation of oxygen consumption [2].
27 472 Minimum heart rates were reached at the bottom of the dive after a period of passive descent
28 473 during “free fall” before showing an overall increase during ascent involving exercise (Figs 2
29 474 & 3B). The inverse relationship between heart rate and depth supports the assumption that
30 475 beyond regulation of HR by the diving response, changes in intrathoracic pressure and lung
31 476 volume may also influence heart rate via a change in activity from pulmonary stretch receptors
32 477 in humans [39] just as in diving mammals [32]. The overall patterns of change in heart rate in
33 478 human freedivers and sea lions, for instance, are strikingly similar (Fig. 3B).

34 479 The magnitude of reduction in heart rate exhibited by the freedivers was pronounced (Fig. 2)
35 480 which is in accordance with earlier reports [40]. As shown in Fig. 4A (red line), where a diver
36 481 exhibits <27 beats over 60 s, sustained exceptionally low heart rates were not uncommon and
37 482 consistent with previous studies of apnoeic cardiovascular responses [41].

38 483 Progressive changes in cardiac waveforms with heart rate and depth – specifically, the
39 484 increased height of the percussive peak (pulse magnitude) and the increased prominence of the
40 485 tidal peak (Fig. 4C) at lower heart rates, were consistent with development of bisfirens pulse.
41 486 Elevated pulse magnitude is indicative of increased blood flow [23] that can be associated with
42 487 phenomena such as high arterial pressure [42] and changes in vascular compliance [43]. The
43 488 prominence of a tidal wave is related to longer and slower systole due to high arterial pressure
44 489 with reduced stroke volume. This is apparent in the relationship between elevated pulse height
45 490 and tidal peak prominence and heart rate – specifically at low heart rates (Fig. 5C). Low heart
46 491 rates displayed by the freedivers are indicative of pronounced arterial restriction. Normally,
47 492 central elastic arteries act to expand and recoil effectively within each cardiac cycle, providing
48 493 a Windkessel effect to dampen hemodynamic pulsatility and facilitate a continuous blood flow
49 494 in the capillaries [44]. However, we speculate that the level of arterial restriction and
50 495 compliance loss at low heart rates <40bpm may lead to a less effective Windkessel function,
51
52
53
54
55
56
57
58
59
60

496 enhancing the high flow, low resistance cerebral pulsatility, thereby generating an increase in
497 percussive peak in the cardiac waveform.

498 Additional information that can be garnered through appropriate signal analysis of NIRS data,
499 as demonstrated here for the human data and transferred to a seal (Fig. 5), could provide
500 insights or open new questions into comparative cardiovascular performance of diving
501 mammals.

502 **Conclusions**

503 Overall, this study demonstrates the ability of CW-NIRS to provide non-invasive and
504 continuous measurement of the patterns of cerebral oxygenation, hemodynamics and cardiac
505 responses of freedivers conducting deep dives. In humans, NIRS has the potential to be an
506 important tool to improve diver's safety. Further, elite human freedivers could act as a tractable
507 diving model as the continuous and high-quality NIRS signal recorded by a single wearable
508 system, served as a proof of principle of CW-NIRS as a physiological measurement tool in a
509 challenging environment. Transferability of signal processing methods, demonstrated here
510 between human diver and seal data, highlights that the NIRS has broader application than only
511 humans, and could begin to help fill knowledge gaps in the diving physiology of free-ranging
512 animals.

513 **References**

- 514 1. Scholander PF. (1940). Experimental investigations on the respiratory function in diving birds
515 and mammals. *Hvaldradets Skr.* 22, 1-31.
- 516 2. Andersson J, Schagatay E. (1998a) Arterial oxygen desaturation during apnea in humans.
517 *Undersea & Hyperbaric Med.* 25, 21-25.
- 518 3. Daly MdB. (2011) Interactions between respiration and circulation. In N. S. Cherhiack & J. G.
519 Widdicombe (Eds.) *Handbook of physiology: The respiratory system II* (pp. 529 – 594).
520 Bethesda, MD: American Physiology Society.
- 521 4. Blix AS, Elsner R, Kjekshus JK. (1983). Cardiac output and its distribution through capillaries
522 and A-V shunts in diving seals. *Acta Physiol. Scand.* 119(2): 109-116.
- 523 5. Blix AS, Folkow B. (1983). Cardiovascular adjustments to diving in mammals and birds. In:
524 Casson DM, Ronald K, editors. *Handbook of Physiology. The Cardiovascular System.*
525 *Peripheral Circulation and Organ Blood Flow.* Bethesda, MD: Am. Physiol. Soc. p. 917-945.
- 526 6. Kooyman GL, Wahrenbrock EA, Castellini MA, Davis RW, Sinnott EE. (1980). Aerobic and
527 anaerobic metabolism during voluntary diving in Weddell seals: Evidence of preferred
528 pathways from blood chemistry and behavior. *J. Comp. Physiol.* 138, 335-346.
- 529 7. Schagatay E, 2011. Review: Predicting performance in competitive apnea diving. Part III:
530 depth. *Diving Hyperbaric Med* 41 (4) 216-228.
- 531 8. Meir JU, Champagne CD, Costa DP, Williams CL, Ponganis PJ. (2009). Extreme hypoxic
532 tolerance and blood oxygen depletion in diving elephant seals. *Am. J. Physiol.* 297(4), 927-
533 939.
- 534 9. McDonald BI, Ponganis PJ. (2013) Insights from venous oxygen profiles: oxygen utilization
535 and management in diving California sea lions, *J. Exp. Biol.* 216, 3332-3341.
- 536 10. Bosco G., Rizzato A., Martani L., Schiavo S., Talamonti E., Garetto G., Paganini M., Camporesi
537 E.M., Moon R.E. 2018. Arterial blood gas analysis in breath-hold divers at depth. *Front.*
538 *Physiol.* 9, 1558.

- 1
2
3 539
4 540
5 541
6 542
7 543
8 544
9 545
10 546
11 547
12 548
13 549
14 550
15 551
16 552
17 553
18 554
19 555
20 556
21 557
22 558
23 559
24 560
25 561
26 562
27 563
28 564
29 565
30 566
31 567
32 568
33 569
34 570
35 571
36 572
37 573
38 574
39 575
40 576
41 577
42 578
43 579
44 580
45 581
46 582
47 583
11. Qvist J, Hurford WE, Park YS, Radermacher P, Falke KJ, Ahn DW, Guyton GP, Stanek KS, Hong SK, Weber RE, Zapol WM. (1993). Arterial blood gas tensions during breath-hold diving in the Korean ama. *J. Appl. Physiol.* 75(1), 285-293.
 12. Zapol WM, Liggins GC, Schneider RC, Qvist J, Snider MT, Creasy RK, Hochachka PW. (1979). Regional blood flow during simulated diving in the conscious Weddell seal. *J. Appl. Physiol.* 47, 968-973.
 13. Davis RD, Kanatous SB. (1999). Convective oxygen transport and tissue oxygen consumption in Weddell seals during aerobic dives. *J. Exp. Biol.* 202, 1091-1113.
 14. Dujic Z, Uglesic L, Breskovic T, Valic Z, Heusser K, Marinovic J, Ljubkovic M, Palanda I. (2009). Involuntary breathing movements improve cerebral oxygenation during apnea struggle phase in elite divers. *J. Appl. Physiol.* 107, 1840 – 1846.
 15. Williams CL, Meir JU, Ponganis PJ. (2011). What triggers the aerobic dive limit? Patterns of muscle oxygen depletion during dives of emperor penguins. *J. Exp. Biol.* 214, 1782-1812.
 16. Fujimoto K, Sano Y. (2014). Applicability of near-infrared spectroscopy for measuring hemodynamics during breath-hold diving. *Jpn. J. Marit. Activity*, 3(1), 24-29.
 17. Williams T, Blackwell SB, Richter B, Sinding M-HS, Heide-Jorgensen MP. (2017). Paradoxical escape responses by narwhals (*Monodon monoceros*). *Science*, 385, 1328-1331.
 18. Fitz-Clarke JR. (2018). Breath-hold diving. *Compr. Physiol.* 8(2), 585-630.
 19. Ferrari, M., & Quaresima, V. (2012). A brief review on the history of human functional near-infrared spectroscopy (fNIRS) development and fields of application. *Neuroimage*, 63(2), 921–935. pmid:22510258
 20. McKnight, J.C., Bennett, K.A., Bronkhorst, M., Russell, D.J.F., Balfour, S., Milne, R., Bivins, M., Moss, S.E.W., Colier, W., Hall, A.J., Thompson, D. (2019). Shining new light on mammalian diving physiology using wearable near-infrared spectroscopy. *PLoS Biol.* 17(6), e3000306
 21. Tisdall MM, Taylor C, Tachtsidis I, Leung TS, Pritchard C, Elwell CE, Smith M. (2009). The effect on cerebral tissue oxygenation index changes in the concentrations of inspired oxygen and end-tidal carbon dioxide in healthy adult volunteers. *Anesth. Analg.* 109(3), 906 – 913.
 22. Menssen J, Colier W, Hopman J, Liem D, de Korte C. (2009). A method to calculate arterial and venous saturation from near-infrared spectroscopy. *Adv. Exp. Med. Biol.* 645, 135-140.
 23. Elgendi M. (2012). On the analysis of fingertip photoplethysmogram signals. *Curr. Cardio. Rev.* 8(1), 14 -25
 24. Suzuki S, Takasaki S, Ozaki T, Kobayashi Y. (1999). A tissue oxygenation monitor using NIR spatially resolved spectroscopy. *Proc. SPIE.* 3597, 582-592.
 25. Al-Rawi PG, Smielewski P, Kirkpatrick PJ. (2001). Evaluation of a near-infrared spectrometer for detection of intracranial oxygenation changes in the adult head. *Stroke.* 32, 2492-2500.
 26. Örnhammar HE, Schagatay E, Andersson J, Bergsten E, Gustafsson P, Sandstrom S. (1998). Mechanisms of 'buccal pumping'. 24th Annual Scientific Meeting, Eur Underwater Baromed Soc, Diving and Hyperbaric Medicine, August 12-15, Stockholm, Sweden, p 80-83.
 27. Hakimi N, Setarehdan SK. (2018). Stress assessment by means of heart rate derived from functional near-infrared spectroscopy. *J. Biomed. Opt.* 23(11), 1.
 28. Scholkmann F, Boss J, Wolf M. (2012). An efficient algorithm for automatic peak detection in noisy periodic and quasi-periodic signals. *Algorithms.* 5(4), 588-603.
 29. Leung TS, Tachtsidis I, Velayuthan P, Oliver C, Henty JR, Jones H, Smith M, Elwell CE, Delpy ST. (2006). Investigation of Oxygen Saturation Derived from Cardiac Pulsations Measured on the Adult Head Using NIR Spectroscopy. In: Cicco G., Bruley D.F., Ferrari M., Harrison D.K.

- 1
2
3 584 (eds) Oxygen Transport to Tissue XXVII. Advances in Experimental Medicine and Biology, vol
4 585 578. Springer, Boston, MA . https://doi.org/10.1007/0-387-29540-2_34
5 586
6 586 30. Franceschini MA, Gratton E, Fantini S. (1999). Noninvasive optical method of measuring
7 587 tissue and arterial saturation: an application to absolute pulse oximetry of the brain. *Optics*
8 588 *Letters*. 24(13), 829-831.
9 589
10 589 31. Sassaroli A, Fantini S. (2004). Comment on the modified Beer-Lambert law for scattering
11 590 media. *Phys. Med. Biol.*, 49 (14), N255–N257.
12 591
13 591 32. McDonald BI, Ponganis PJ. (2014). Deep-diving sea lions exhibit extreme bradycardia in long
14 592 duration dives, *J. Exp. Biol.* 217, 1525 – 1524 (2014).
15 593
16 593 33. Novalija J, Lindholm P, Loring SH, Diaz E, Fox JA, Ferrigno M. (2007). Cardiovascular aspects
17 594 of glossopharyngeal insufflation and exsufflation. *Undersea and Hyperbaric Medicine*. 34(6),
18 595 415-423.
19 596
20 596 34. Eichhorn L, Erdfelder F, Kessler F, Doerner J, Thudium MO, Meyer R, Ellerkmann RK. (2015).
21 597 Evaluation of near-infrared spectroscopy under apnea-dependent hypoxia in humans. *J Clin*
22 598 *Monit Comput.* 29(6), 749-57. doi: 10.1007/s10877-015-9662-2. Epub 2015 Feb 4. PMID:
23 599 25649718.
24 600
25 600 35. Eichhorn L, Doerner J, Luetkens JA, Lunkenheimer JM, Dolscheid-Pommerich RC, Erdfelder F,
26 601 Fimmers R, Nadal J, Stoffel-Wagner B, Schild HH, Hoeft A, Zur B, Naehle CP. (2018).
27 602 Cardiovascular magnetic resonance assessment of acute cardiovascular effects of voluntary
28 603 apnoea in elite divers. *J Cardiovasc Magn Reson.* 20(1), 40. doi: 10.1186/s12968-018-0455-x
29 604
30 604 36. Grocott MPW, Martin DS, Levett DZH, McMorrow R, Windsor J, Montgomery H. (2009).
31 605 Arterial blood gases and oxygen content in climbers on mount Everest. *N. Engl. J. Med.* 360,
32 606 140-149.
33 607
34 607 37. Nolet BA, Butler PJ, Masman D, Woakes AJ. (1992). Estimation of daily energy expenditure
35 608 from heart rate and doubly labelled water in exercising geese. *Physiological Zoology*. 65(6),
36 609 1188-1216.
37 610
38 610 38. Lemaître F, Lafay v, Taylor M, Costalat G and Gaedette B. (2013). Electrocardiographic
39 611 aspects of deep diving in elite breath-hold divers. *Undersea Hyperb. Med.* 40(2), 145 – 154.
40 612
41 612 39. Andersson J, E Schagatay (1998b) Effects of lung volume and involuntary breathing
42 613 movements on the human diving response. *Eur J Appl Physiol* 77: 19-24.
43 614
44 614 40. Ferretti G. (2001). Extreme human breath-hold diving. *Eur J Appl Physiol.* 84, 254-271.
45 615
46 615 41. Lindholm P, Sundblad P, Linnarsson D. (1999). Oxygen-conserving effects of apnea in
47 616 exercising men. *J. Appl. Physiol.* 87(6), 2122-2127.
48 617
49 617 42. Xing X, Sun M. (2016). Optical blood pressure estimation with photoplethysmography and
50 618 FFT-based neural networks. *Biomed. Opt. Express*, 7(8), 3007-3020.
51 619
52 619 43. O'Rourke MF, Nichols WW. (2005). Aortic diameter, aortic stiffness, and wave reflection
53 620 increase with age and isolated systolic hypertension. *Hypertension*, 45, 652-658.
54 621
55 621 44. Nichols WW, O'Rourke MF. McDonald's blood flow in arteries. New York: Oxford University
56 622 Press; 2005.

54 623 **Acknowledgements:** We thank the elite freedivers for their kind cooperation, and Mr Marick Le
55 624 Hérissé for help to carry out this study. We thank Mr Sean McHugh and Mr Philippe Hubert for
56 625 assistance in the construction of the PortaDiver and Mr Simon Moss and Mr Ryan Milne for their
57 626 roles in performing animal experiments. **Author Contributions: J. Chris McKnight:**
58 627 Conceptualisation, Methodology, Software, Formal analysis, Investigation, Data Curation,
59 628 Writing, Visualisation. **Eric Mulder:** Investigation, Writing – Review and Editing, Project

1
2
3 629 administration. **Alexander Ruesch:** Software, Formal analysis, Investigation, Visualisation,
4 630 Writing. **Jana Kainerstorfer:** Conceptualisation, Methodology, Software, Writing. **Nasar**
5 631 **Hakimi:** Software, Writing – Original Draft. **Jingyi Wu:** Software, Formal Analysis, Writing
6 632 Original Draft. **Steve Balfour:** Methodology, Resources, Writing – Review and Editing. **Mathijs**
7 633 **Bronkhorst:** Methodology, Resources, Writing. **Jörn M. Horschig:** Software, Formal analysis,
8 634 Resources and Writing - Review and Editing. **Frank Parnett:** Data interpretation and writing.
9 635 **Katsufumi Sato:** Resources and Writing – Review and Editing. **Gordon D. Hastie:** Resources,
10 636 Writing – Review and Editing, and Funding acquisition (seal data). **Peter Tyack:** Resources and
11 637 Writing – Original Draft. **Erika Schagatay:** Conceptualization, Resources and contacts, Data
12 638 interpretation and Writing, Project Administration and Funding acquisition (human data).
13 639 **Funding:** Human data were funded by the Jennifer and Peter Francis Donation, by Swedish Centre
14 640 for Research in Sports and Mid-Sweden University. Grey seal NIRS data were funded as part of
15 641 the Department for Business, Energy and Industrial Strategy Offshore Energy Strategic
16 642 Environmental Assessment programme. **Competing interests:** Authors declare no competing
17 643 interest. Funders had no involvement in study design, data collection or manuscript preparation.
18 644 **Data and materials availability:** Seal data can be provided, but please note that human data cannot
19 645 be provided due to conflict with Ethical approval.
20
21
22
23
24
25
26
27
28
29
30
31
32
33
34
35
36
37
38
39
40
41
42
43
44
45
46
47
48
49
50
51
52
53
54
55
56
57
58
59
60

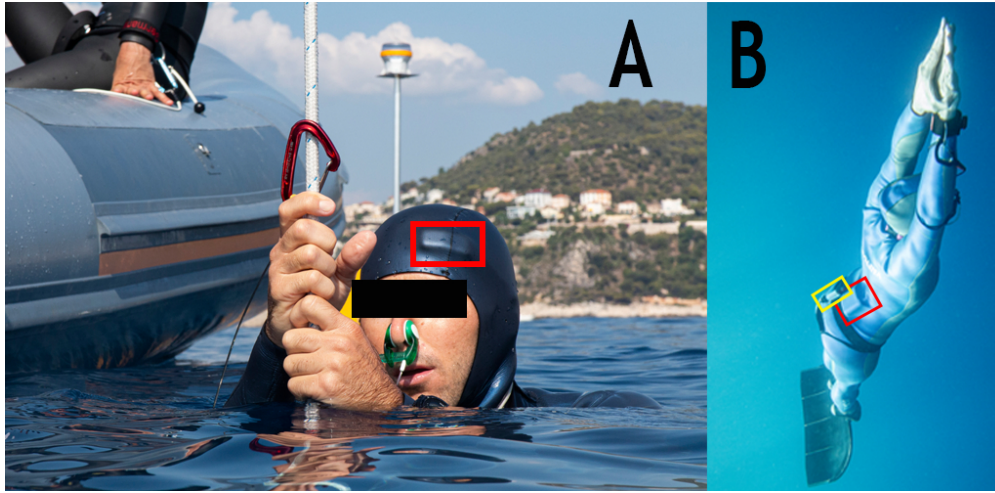


Fig. 1. Monitoring diving physiology and behaviour in elite freedivers. (A) Location of NIRS sensor-head over prefrontal cortex (red box). (B) Respective placements of NIRS sensor body (red box) and Little Leonardo W1000-PD3GT (yellow box).

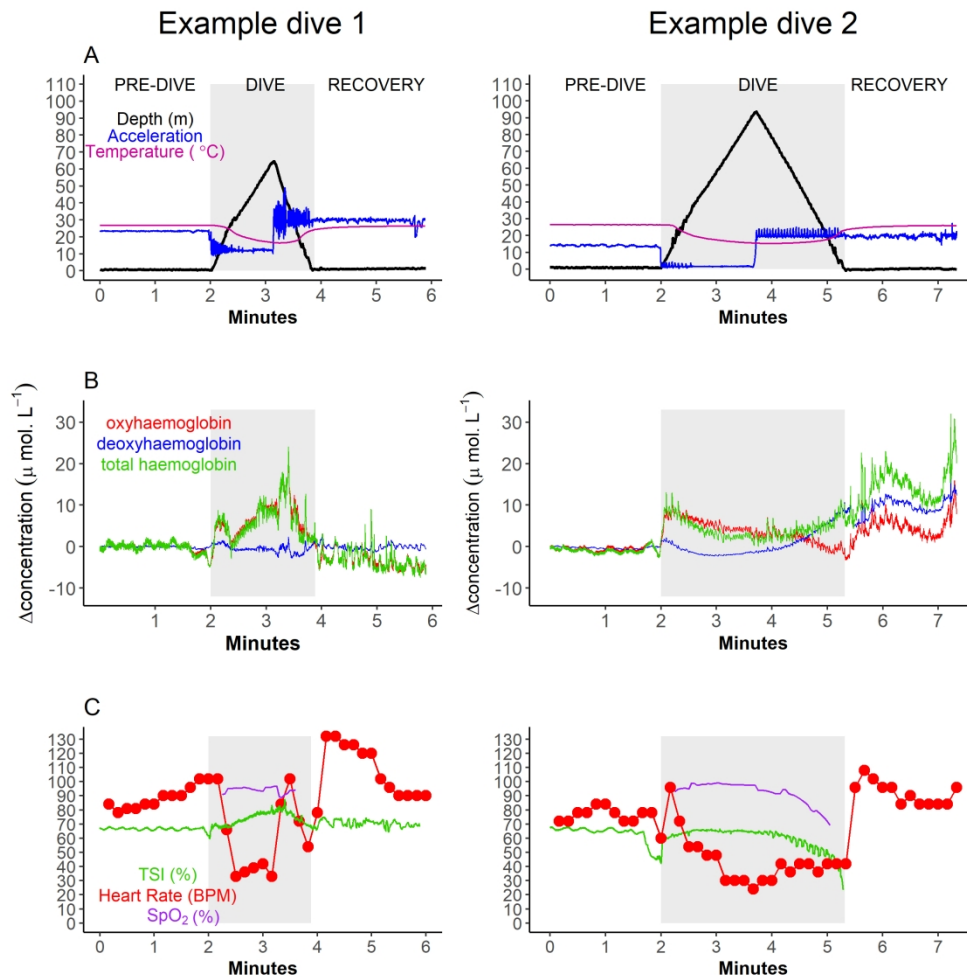


Fig. 2. Monitoring physiological variables in freedivers. Two example dives to 67 m and 97 m from two freedivers, showing (A) Dive and temperature data (B) Cerebral hemodynamic responses. (C) Heart rate, cerebral and arterial blood oxygen responses. High-frequency peaks and troughs in the accelerometry signal are indicative of leg movements associated with swimming in the CWT dive in example 1 and arm movements of pulling along the rope in a FIM dive in example 2. During early descent the divers swim intensely to overcome positive buoyancy which is seen as high amplitude peaks on the acceleration trace, while later during the descent the negatively buoyant divers free-fall. At the bottom of the dive when the divers turn and swim upwards against negative buoyancy, the acceleration trace, again, shows high amplitude peaks throughout ascent. Oscillations in TSI from minutes 4 to 5 in example 2 were likely the result of involuntary breathing movements [14]. TSI measurement in example 2 was lost on surfacing as one of three NIRS channels lost contact with the diver's head.

228x228mm (300 x 300 DPI)

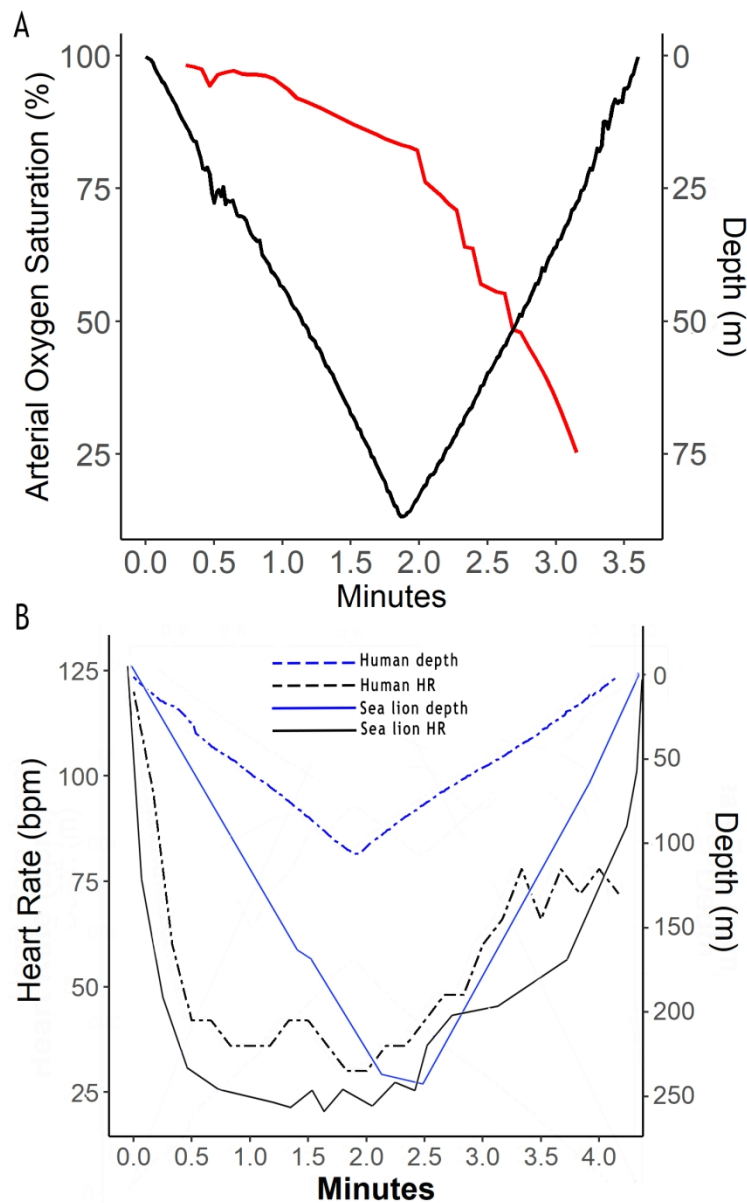


Fig. 3. (A) Arterial oxygen saturation (SpO_2) and depth data from a dive resulting in the lowest arterial blood oxygenation recorded (25%). (B) Heart rate and depth profiles for a human diver (80kg) perform the deepest dive recorded (107 m) and an 81 kg California sea lion (*Zalophus californianus*) diving to 240 m (data re-drawn with permission from McDonald and Ponganis 2014 [32])

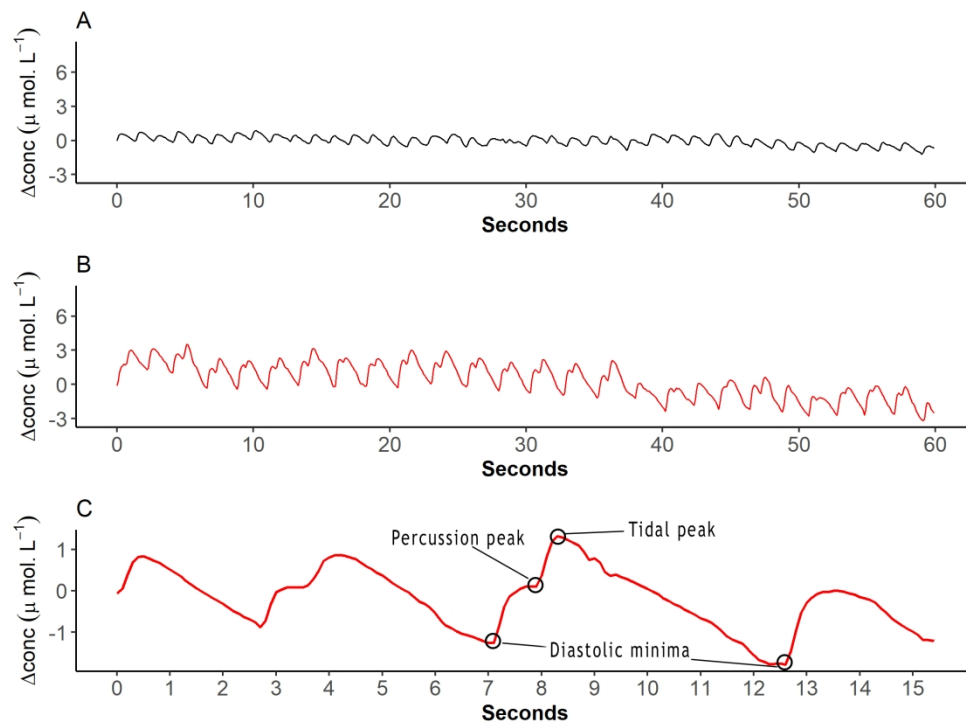
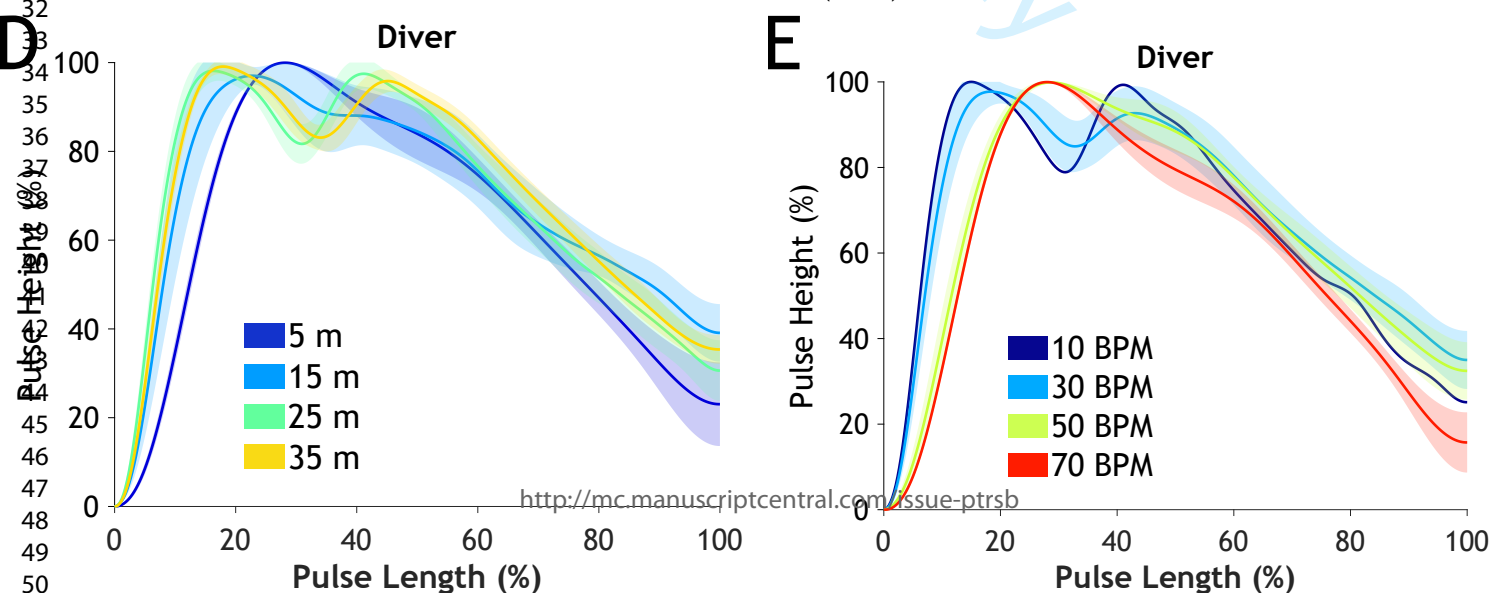
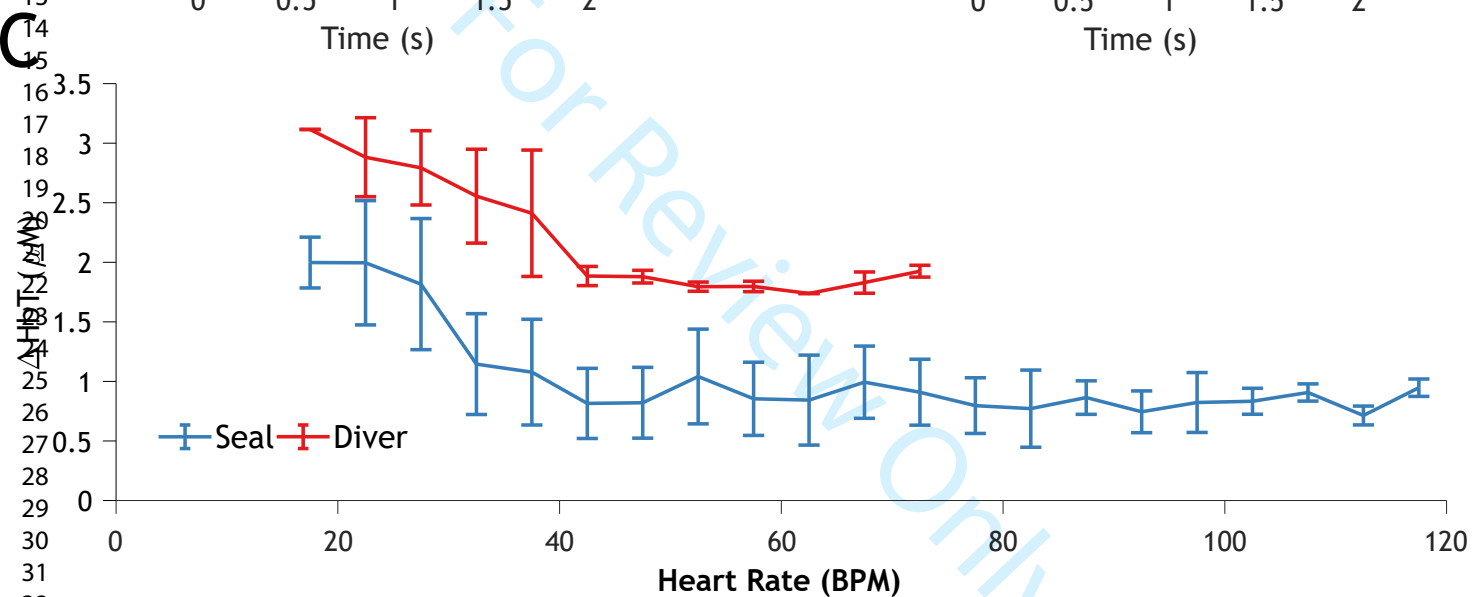
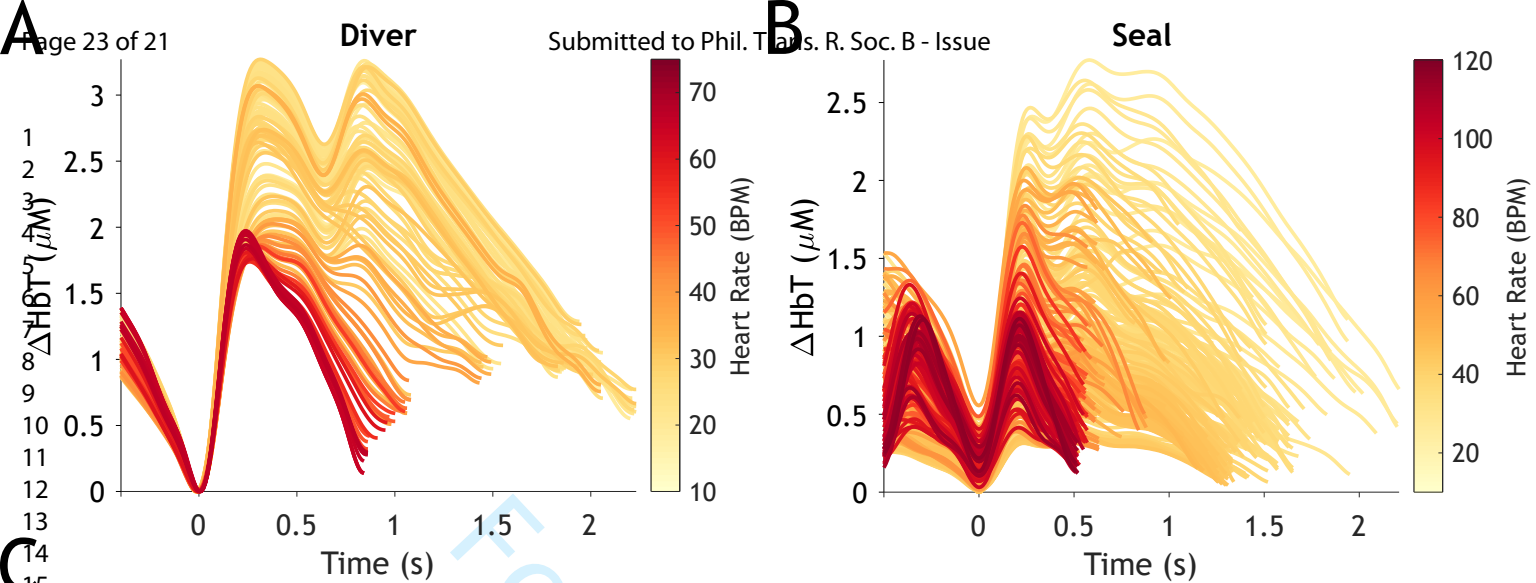


Fig. 4. Raw [O₂Hb] traces visualising heart rate and cardiac waveform. (A) Shape and magnitude of a normal cardiac waveform at 41bpm. (B) Cardiac waveform with increased magnitude and pronounced tidal waves at a heart rate of 27bpm. (C) Cardiac waveforms across four cardiac cycles with three key features identified – (1) percussive wave (originating from the contraction of the left ventricle and ejection of blood); (2) tidal wave (caused by the elasticity of aortic wall); (3) diastolic minimum (caused by relaxation of heart) - showing the transient changes in cardiac waveform on the longest interbeat interval (5.4 s) recorded.

203x152mm (300 x 300 DPI)



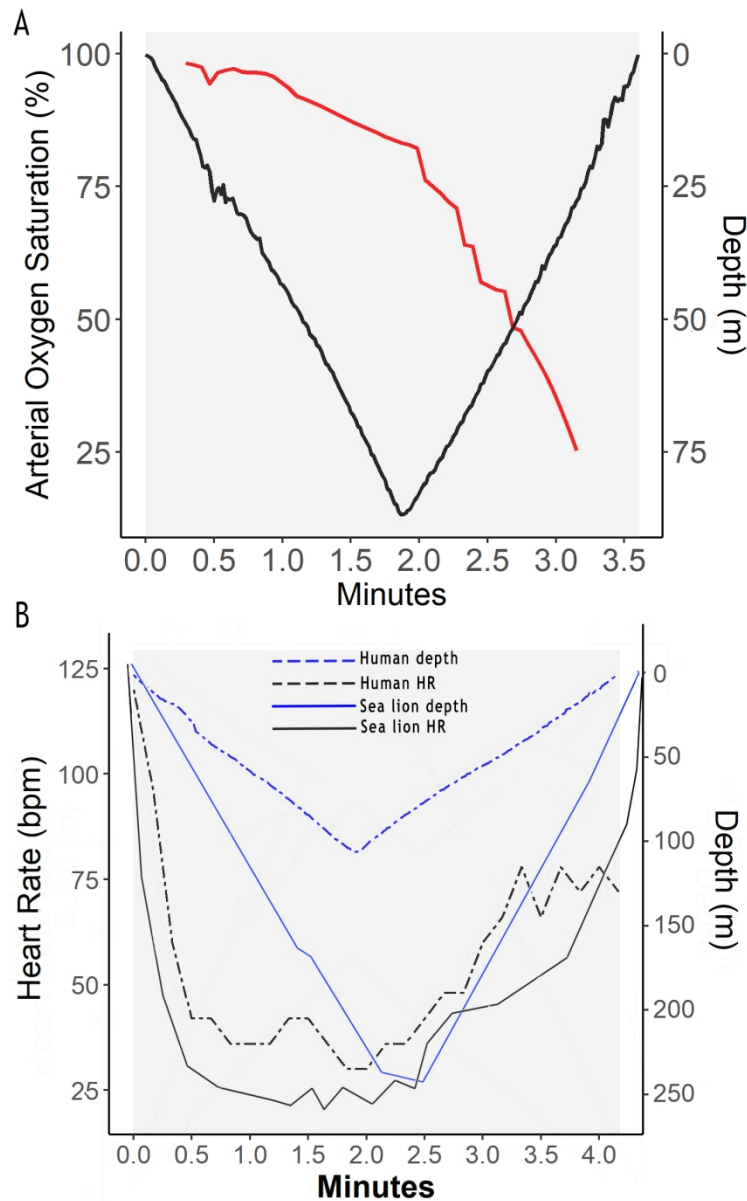


Fig. 3. (A) Arterial oxygen saturation (SpO_2) and depth data from a dive resulting in the lowest arterial blood oxygenation recorded (25%). (B) Heart rate and depth profiles for a human diver (80kg) perform the deepest dive recorded (107 m) and an 81 kg California sea lion (*Zalophus californianus*) diving to 240 m (data re-drawn with permission from McDonald and Ponganis 2014 [32]). Shaded grey areas in A and B indicate the diving periods for human divers.